ρ meson form factors in a confining Nambu–Jona-Lasinio model

Manuel E. Carrillo-Serrano,[1] Wolfgang Bentz,[2] Ian C. Cloët,[3] and Anthony W. Thomas[1]

[1]*CSSM and ARC Centre of Excellence for Particle Physics at the Tera-scale,*
Department of Physics, University of Adelaide, Adelaide, South Australia 5005, Australia
[2]*Department of Physics, School of Science, Tokai University, 4-1-1 Kitakaname, Hiratsuka-shi, Kanagawa 259-1292, Japan*
[3]*Physics Division, Argonne National Laboratory, Argonne, Illinois 60439, USA*

Elastic electromagnetic form factors for the ρ^+ meson are calculated in a Nambu–Jona-Lasinio model which incorporates quark confinement through the use of the proper-time regularization scheme. A comparison is made with recent lattice QCD results and previous quark model calculations for static quantities and the Sachs form factors. The results are qualitatively in good agreement with the lattice QCD calculations, with the exception of the quadrupole moment and corresponding form factor, which may be related to a lack of spherical symmetry on the lattice.

I. INTRODUCTION

The structure of hadrons presents a remarkable challenge to the theory of strong interactions—quantum chromodynamics (QCD)—and a critical feature of a hadron's structure is its distribution of charge and magnetization, which is empirically related to its electromagnetic form factors [1]. The direct calculation of hadron form factors using QCD is currently only possible through lattice QCD, albeit limited to the low to moderate Q^2 region. However, to gain insight into the relevant dynamical mechanisms behind the observed structure it is useful to work with models that approximate key features of QCD. An important focus for this comparison are the meson form factors. Because of their short lifetimes [2] they present a unique challenge experimentally—making both lattice QCD and model calculations critical. The pion form factor has been successfully measured over a wide range of four-momentum transfer, while the vector meson form factors have not had the same amount of experimental exploration. However, the BABAR Collaboration has measured the cross section for the reaction $e^+ + e^- \rightarrow \rho^+ + \rho^-$ [3], which has been analyzed to garner information on the ρ meson form factors [4].

The ρ form factors, or equivalently the polarization amplitudes, have been calculated using a variety of methods, for example, phenomenological models [5,6], constituent quark models in the light front [7–13] and point form [14] frameworks, QCD sum rules [15–18], and the Dyson-Schwinger equations [19–22]. The first attempts to compute ρ form factors using lattice QCD were reported in Refs. [23,24] in the quenched framework. The recent work of Owen *et al.* [25] and Shultz *et al.* [26] give two independent lattice QCD calculations based upon different approaches. These lattice results, and the previous work with quark models, provide a solid background for comparison with results computed within other models.

In this work we extend the ρ meson form factor calculation of Ref. [27], where the focus was a comparison with the axial-vector diquark form factors which formed a critical part of a nucleon form factor calculation. Here we use the same confining version of the Nambu–Jona-Lasinio (NJL) model [28,29] to investigate the quark mass dependence of the ρ form factors, and perform a detailed comparison with the lattice QCD results of Refs. [25,26]. Following Ref. [27] we include the dressing of the quark-photon vertex from the inhomogeneous Bethe-Salpeter equation and a pion cloud, which are critical for obtaining a good agreement with lattice results. Similar finding were made in Ref. [30], where the same framework was applied to the π and K form factors.

The outline of the paper is as follows: In Sec. II we briefly review the NJL model as applied to $\bar{q}q$ bound states, and the calculation of the ρ electromagnetic form factors is discussed in Sec. III. The results are compared to those from lattice QCD and various quark models in Sec. IV, and Sec. V presents our conclusions.

II. NAMBU–JONA-LASINIO MODEL

In its original formulation the NJL model successfully encapsulated the effects of dynamical chiral symmetry breaking, where the pion emerged as a Goldstone boson and the nucleon was the fundamental degree of freedom [28,29]. The NJL model has subsequently been re-expressed with quarks as the fundamental constituents, making the relation with QCD evident. Importantly, the NJL model [31] preserves the fundamental symmetries of QCD. In particular, the generation of mass through the dynamical breaking of chiral symmetry is beautifully illustrated. In contrast, quark confinement is not automatically incorporated in the model. However, it has been shown that it can be mimicked by the introduction of an infrared cutoff in the proper-time regularization scheme [32–34]. The NJL model has a history of success in the description of numerous meson [31,35,36] and baryon [35,36] properties, including the nucleon parton distribution functions [37–41] and electromagnetic form factors [27]. More recently these studies have been extended to the computation of the axial charges for strangeness conserved β decays in the baryon octet [42] and possible insights into the solutions of long time enigmas in QCD, such as the $\Delta I = 1/2$ rule in kaon decays [43]. It is this wealth of achievement, together with the recent developments in lattice QCD, that encourages us to test
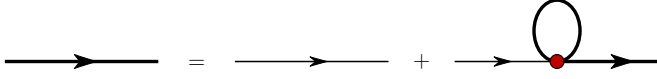
FIG. 1. (Color online) NJL gap equation in the Hartree-Fock approximation, where the thin line represents the elementary quark propagator, $S_0^{-1}(k) = \not{k} - m + i\varepsilon$, and the shaded circle represents the four-fermion interaction.

whether the model gives an accurate description of ρ meson properties.

In the application of the NJL model to the solution of the form factors of the ρ meson, we use a two-flavor NJL Lagrangian which in the $\bar{q}q$ interaction channel reads:

$$\mathcal{L} = \bar{\psi}(i\not{\partial} - \hat{m})\psi + \frac{1}{2}G_\pi[(\bar{\psi}\psi)^2 - (\bar{\psi}\gamma_5\vec{\tau}\psi)^2]$$
$$- \frac{1}{2}G_\omega(\bar{\psi}\gamma^\mu\psi)^2 - \frac{1}{2}G_\rho[(\bar{\psi}\gamma^\mu\vec{\tau}\psi) + (\bar{\psi}\gamma^\mu\gamma_5\vec{\tau}\psi)^2], \tag{1}$$

where $\vec{\tau}$ are the Pauli matrices representing isospin and $\hat{m} = \mathrm{diag}[m_u, m_d]$ is the current quark mass matrix. We assume $m_u = m_d = m$. The fermion coupling G_π represents the strength of the scalar ($\bar{q}q$) and pseudoscalar ($\bar{q}\gamma_5 q$) interaction channels and is responsible for the dynamical generation of the dressed quark masses through the breaking of chiral symmetry. The strength of the vector-isoscalar and vector-isovector four-fermion interactions is given by G_ω and G_ρ, respectively. The explicit breaking of $U(1)$ axial symmetry is often modeled by the inclusion of an extra six-fermion determinant interaction term, which describes the η and η' mass splitting [31]; however, this is not directly related to our calculation so we do not consider it. We regularize the NJL interaction through the proper-time regularization scheme, using an infrared cutoff (Λ_{IR}) to remove unphysical decay thresholds for hadrons into quarks [32–34].

The dressed quark masses are given by the solution of the gap equation depicted in Fig. 1, which in the proper-time scheme reads

$$M = m + \frac{3}{\pi^2}M\,G_\pi\int_{1/\Lambda_{UV}^2}^{1/\Lambda_{IR}^2}d\tau\,\frac{e^{-\tau M^2}}{\tau^2}, \tag{2}$$

giving a dressed quark propagator of the form:

$$S(k)^{-1} = \not{k} - M + i\varepsilon. \tag{3}$$

The description of mesons as $\bar{q}q$ bound states in the NJL model is obtained via the Bethe-Salpeter equation (BSE) in the random-phase approximation, as illustrated in Fig. 2. The
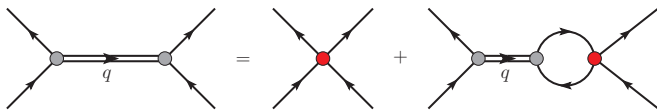

FIG. 2. (Color online) Bethe-Salpeter equation for antiquark-quark (meson) correlations in the NJL model using the random phase approximation.

solution of the BSE in each meson channel is given by a two-body t matrix that depends on the nature of the interaction channel [27], where the reduced t matrices for the π, ρ, and ω mesons read

$$\tau_\pi(q) = \frac{-2i\,G_\pi}{1 + 2\,G_\pi\,\Pi_{PP}(q^2)}, \tag{4}$$

$$\tau_{\rho(\omega)}^{\mu\nu}(q) = \frac{-2i\,G_{\rho(\omega)}}{1 + 2\,G_{\rho(\omega)}\,\Pi_{VV}(q^2)}$$
$$\times\left[g^{\mu\nu} + 2\,G_{\rho(\omega)}\,\Pi_{VV}(q^2)\frac{q^\mu q^\nu}{q^2}\right], \tag{5}$$

and the bubble diagrams are defined by

$$\Pi_{PP}(q^2) = 6i\int\frac{d^4k}{(2\pi)^4}\,\mathrm{Tr}_D[\gamma_5\,S(k)\,\gamma_5\,S(k+q)], \tag{6}$$

$$\Pi_{VV}(q^2)\left(g^{\mu\nu} - \frac{q^\mu q^\nu}{q^2}\right)$$
$$= 6i\int\frac{d^4k}{(2\pi)^4}\,\mathrm{Tr}_D[\gamma^\mu\,S(k)\,\gamma^\nu\,S(k+q)]. \tag{7}$$

The meson masses are given by the poles in the reduced t matrices, that is,

$$1 + 2\,G_\pi\,\Pi_{PP}(q^2 = m_\pi^2) = 0, \tag{8}$$

$$1 + 2\,G_\rho\,\Pi_{VV}(q^2 = m_\rho^2) = 0, \tag{9}$$

$$1 + 2\,G_\omega\,\Pi_{VV}(q^2 = m_\omega^2) = 0. \tag{10}$$

Expanding the full t matrices about these poles gives the homogeneous Bethe-Salpeter vertices for the π, ρ, and ω mesons:

$$\Gamma_\pi^i = \sqrt{Z_\pi}\,\gamma_5\,\tau_i, \quad \Gamma_\rho^{\mu,i} = \sqrt{Z_\rho}\,\gamma^\mu\,\tau_i, \quad \Gamma_\omega^\mu = \sqrt{Z_\omega}\,\gamma^\mu, \tag{11}$$

where the meson-quark-quark couplings read [30,31,36]

$$Z_\pi^{-1} = -\frac{\partial}{\partial q^2}\,\Pi_{PP}(q^2)\Big|_{q^2=m_\pi^2}, \tag{12}$$

$$Z_{\rho(\omega)}^{-1} = -\frac{\partial}{\partial q^2}\,\Pi_{VV}(q^2)\Big|_{q^2=m_{\rho(\omega)}^2}. \tag{13}$$

III. ρ ELECTROMAGNETIC FORM FACTORS

The electromagnetic current for a ρ meson is parametrized by three form factors and takes the form

$$j_\rho^{\mu,\alpha\beta}(p',p) = \left[g^{\alpha\beta}F_{1\rho}(Q^2) - \frac{q^\alpha q^\beta}{2m_\rho^2}F_{2\rho}(Q^2)\right](p'+p)^\mu$$
$$- (q^\alpha g^{\mu\beta} - q^\beta g^{\mu\alpha})F_{3\rho}(Q^2), \tag{14}$$

where the polarizations of the incoming and outgoing ρ mesons are represented by the Lorentz indices α and β, respectively, and μ is the photon polarization. From these form factors one can define three Sachs form factors for the ρ, namely, the charge [$G_C(Q^2)$], magnetic [$G_M(Q^2)$], and quadrupole [$G_Q(Q^2)$] form factors, which read

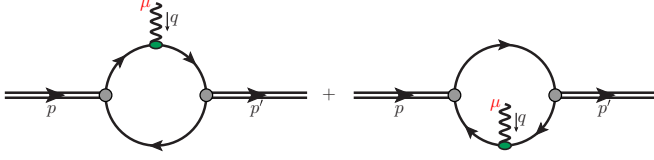$$G_C(Q^2) = F_1(Q^2) + \frac{2}{3}\eta\,G_Q(Q^2), \tag{15}$$

FIG. 3. (Color online) Feynman diagrams representing the electromagnetic current for a meson in our NJL model.

FIG. 5. (Color online) Pion cloud contribution to the quark-photon vertex. The quark-photon interaction in the first two diagrams, represented by the shaded ovals, is given by the solution of the inhomogeneous BSE. The last diagram also includes the pion form factor determined without the pion cloud on the associated dressed quarks.

$$G_M(Q^2) = F_3(Q^2), \tag{16}$$

$$G_Q(Q^2) = F_1(Q^2) + (1 + \eta) F_2(Q^2) - F_3(Q^2), \tag{17}$$

where $\eta = \frac{Q^2}{4 m_\rho^2}$ and all form factors are dimensionless.

In our NJL model the ρ electromagnetic current is depicted in Fig. 3 and expressed by

$$
\begin{aligned}
&j_{\rho,ij}^{\mu,\alpha\beta}(p',p) \\
&= i \int \frac{d^4k}{(2\pi)^4} \mathrm{Tr}\big[\overline{\Gamma}_\rho^{\beta,j} S(p'+k) \Lambda^\mu(p',p) S(p+k) \Gamma_\rho^{\alpha,i} S(k)\big] \\
&\quad + i \int \frac{d^4k}{(2\pi)^4} \mathrm{Tr}\big[\Gamma_\rho^{\alpha,i} S(k-p) \Lambda^\mu(p',p) S(k-p')\overline{\Gamma}_\rho^{\beta,j} S(k)\big],
\end{aligned}
\tag{18}
$$

where the Bethe-Salpeter vertices for the ρ are given in Eq. (11), $\Lambda^\mu(p,p')$ is the dressed quark-photon vertex, and the trace is over Dirac, color, and isospin indices. Following the calculations in Refs. [27,30], we consider three versions of the quark-photon vertex, each of increasing sophistication: a pointlike quark-photon vertex, a vertex given by the solution of the inhomogeneous Bethe-Salpeter equation (illustrated in Fig. 4), and finally a quark-photon vertex which includes the pion cloud at the quark level (see Fig. 5).

The pointlike quark photon is simply given by

$$\Lambda^{(\mathrm{PL})\mu}(p,p') = \left[\frac{1}{6} + \frac{\tau_3}{2}\right]\gamma^\mu, \tag{19}$$

where $\frac{1}{6} + \frac{\tau_3}{2}$ is the quark charge operator. Projecting onto flavor sectors the vertex is separated into two components:

$$\Lambda^{(\mathrm{PL})\mu}(p,p') = \left[e_u \frac{1+\tau_3}{2} + e_d \frac{1-\tau_3}{2}\right]\gamma^\mu, \tag{20}$$

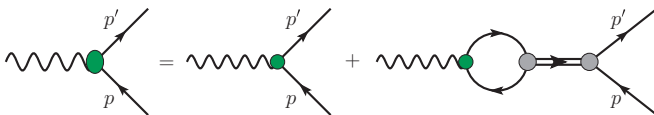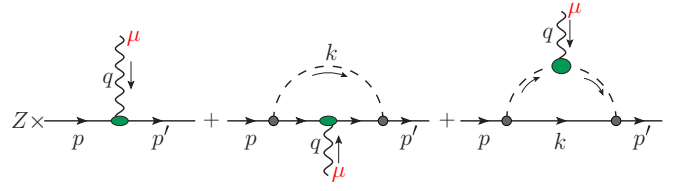where e_u and e_d are the charges of the u and d quarks, respectively.

FIG. 4. (Color online) Inhomogeneous BSE whose solution gives the quark-photon vertex, represented as the large shaded oval. The small circle depicts the pointlike quark-photon driving term of Eq. (19), whereas the shaded circles with the double line represents the vector meson t matrices.

In general the quark-photon vertex is dressed by $\bar{q}q$ interactions in the vector channel, and in the NJL model this dressing is described by the corresponding inhomogeneous Bethe-Salpeter equation (see Fig. 4). From the NJL Lagrangian of Eq. (1) the contributions to this vertex come from the neutral vector mesons (ρ^0 and ω). In the on-shell approximation for the external quarks, the solution of the inhomogeneous Bethe-Salpeter equation of Fig. 4 is

$$\Lambda^{(\mathrm{BSE})\mu}(p,p') = \left[\frac{1}{6} F_{1\omega}(q^2) + \frac{\tau_3}{2} F_{1\rho}(q^2)\right]\gamma^\mu, \tag{21}$$

where the dressed quark form factors are

$$F_{1\omega(\rho)}(q^2) = \frac{1}{1 + 2 G_{\omega(\rho)} \Pi_{VV}(q^2)}. \tag{22}$$

Note, with the Lagrangian of Eq. (1) the inhomogeneous Bethe-Salpeter equation does not generate a Pauli form factor for the dressed quarks. Again projecting into flavor sectors gives

$$\Lambda^{(\mathrm{BSE})\mu}(p,p') = \left[F_{1U}^{\mathrm{BSE}}(q^2)\frac{1+\tau_3}{2} + F_{1D}^{\mathrm{BSE}}(q^2)\frac{1-\tau_3}{2}\right]\gamma^\mu, \tag{23}$$

where the dressed quark form factors are given by [27]

$$F_{1U}^{\mathrm{BSE}}(Q^2) = \tfrac{1}{6} F_{1\omega}(Q^2) + \tfrac{1}{2} F_{1\rho}(Q^2), \tag{24}$$

$$F_{1D}^{\mathrm{BSE}}(Q^2) = \tfrac{1}{6} F_{1\omega}(Q^2) - \tfrac{1}{2} F_{1\rho}(Q^2). \tag{25}$$

Finally we include pion loop corrections to the quark-photon vertex, as illustrated in Fig. 5, which give a vertex of the form

$$\Lambda^\mu(p,p') = \Lambda_U^\mu(p,p')\frac{1+\tau_3}{2} + \Lambda_D^\mu(p,p')\frac{1-\tau_3}{2}, \tag{26}$$

where the flavor sector vertices ($Q = U, D$) read

$$\Lambda_Q^\mu(p,p') = \gamma^\mu F_{1Q}(q^2) + \frac{i\sigma^{\mu\mu}q_\nu}{2 M} F_{2Q}(Q^2). \tag{27}$$

Note that the pion cloud generates a Pauli form factor for the dressed quarks and that in obtaining Eq. (27) we have assumed the external quark lines are on-shell. The dressed quark form

factors now read [27]

$$F_{1U} = Z\left[\tfrac{1}{6}F_{1\omega} + \tfrac{1}{2}F_{1\rho}\right] + [F_{1\omega} - F_{1\rho}]f_1^q + F_{1\rho}f_1^\pi, \quad (28)$$

$$F_{1D} = Z\left[\tfrac{1}{6}F_{1\omega} - \tfrac{1}{2}F_{1\rho}\right] + [F_{1\omega} + F_{1\rho}]f_1^q - F_{1\rho}f_1^\pi, \quad (29)$$

$$F_{2U} = [F_{1\omega} - F_{1\rho}]f_2^q + F_{1\rho}f_2^\pi, \quad (30)$$

$$F_{2D} = [F_{1\omega} + F_{1\rho}]f_2^q - F_{1\rho}f_2^\pi, \quad (31)$$

where for clarity we have dropped the explicit Q^2 dependence. The renormalization factor Z is given by

$$Z = 1 + \left.\frac{\partial \Sigma(p)}{\partial \not{p}}\right|_{\not{p}=M}, \quad (32)$$

where $\Sigma(p)$ is the self-energy from the pion cloud on a dressed quark:

$$\Sigma(p) = -\int \frac{d^4k}{(2\pi)^4}\, \gamma_5\, \tau_i\, S(p-k)\, \gamma_5\, \tau_i\, \tau_\pi(k). \quad (33)$$

Here the pion propagator is approximated by its pole form

$$\tau_\pi(k) \to \frac{i\,Z_\pi}{p^2 - m_\pi^2 + i\epsilon}. \quad (34)$$

The contributions of the pion cloud to the quark-photon vertex are contained in the functions $f_i^q(Q^2)$ and $f_i^\pi(Q^2)(i = 1,2)$ of Eqs. (28)–(31). These body form factors are associated with the second and third diagrams in Fig. 5, which are respectively expressed as

$$\Lambda_Q^{(q)\mu}(p',p) = \gamma^\mu f_1^q(q^2) + \frac{i\sigma^{\mu\nu}q_\nu}{2M} f_2^q(q^2), \quad (35)$$

$$\Lambda_Q^{(\pi)\mu}(p',p) = \gamma^\mu f_1^\pi(q^2) + \frac{i\sigma^{\mu\nu}q_\nu}{2M} f_2^\pi(q^2). \quad (36)$$

The analytic expressions read

$$\Lambda_Q^{(q)\mu}(p',p) = \int \frac{d^4k}{(2\pi)^4}\, \gamma_5\, iS(p'-k)\gamma^\mu\, iS(p-k)\gamma_5\, \tau_\pi(k), \quad (37)$$

$$\Lambda_Q^{(\pi)\mu}(p',p) = Z_\pi^{-1}\,(p'+p)^\mu\, F_\pi^{(\mathrm{PL})}(q^2)$$
$$\times \int \frac{d^4k}{(2\pi)^4}\, \gamma_5\, \tau_\pi(p'-k)\, \tau_\pi(p-k)\, \gamma_5\, iS(k), \quad (38)$$

where $F_\pi^{(\mathrm{PL})}(q^2)$ is the pion form factor determined with a pointlike quark-photon vertex.

For the full calculation of the ρ meson form factors we use Eq. (18) and the quark-photon vertex given in Eq. (26). For the ρ^+ form factors this gives

$$F_{i\rho^+}(Q^2) = [F_{1U}(Q^2) - F_{1D}(Q^2)]f_i^V(Q^2)$$
$$+ [F_{2U}(Q^2) - F_{2D}(Q^2)]f_i^T(Q^2), \quad (39)$$

where $i = 1,2,3$ indicates each of the three form factors of Eq. (14). The body form factors f_i^V are associated with the vector part (γ^μ) of the quark-photon vertex in Eq. (27), while f_i^T are the body form factors associated with the tensor coupling ($\frac{i\sigma^{\mu\nu}q_\nu}{2M}$) in Eq. (27). To obtain the ρ meson

form factors that result only from the inhomogeneous BSE quark-photon vertex we then simply set $Z = 1$ and the pion cloud contributions [$f_1^q(Q^2)$, $f_1^\pi(Q^2)$, etc.] to zero. Finally, the ρ form factors for a pointlike quark-photon vertex are then obtained by setting $F_{1\omega} = F_{1\rho} = 1$. Note, all loop integrals are regularized using the proper-time scheme, with both an infrared and ultraviolet cutoff, except those of Eqs. (33), (37), and (38), where we take the infrared cutoff (Λ_{IR}) to zero because the pion should not be confined.

IV. RESULTS

The parameters of our model are the dressed quark mass M; the regularization cutoffs Λ_{UV} and Λ_{IR}; and the Lagrangian couplings G_π, G_ρ, and G_ω. For consistency with previous work we set $M = 0.4$ GeV (in the physical limit: $m_\pi = 140$ MeV) and $\Lambda_{\mathrm{IR}} = 0.24$ GeV [27,30,42]. The ultraviolet cutoff Λ_{UV} is fit to the physical value of the pion decay constant and the couplings G_π, G_ρ, and G_ω are fit to the physical masses of the π, ρ, and ω mesons using Eqs. (8)–(10). The values of these parameters, together with the quark-meson couplings of Eqs. (12) and (13), are given in Table I.

Our purpose here is to compare results within this NJL model with other calculations, for example, constituent quark models [6–14], QCD sum rules [15–18], Dyson-Schwinger equations [19–22], and the recent lattice QCD studies [25,26]. We first focus on static electromagnetic quantities for the ρ^+ meson and consider the magnetic moment (μ_ρ), quadrupole moment ($\mathcal{Q}_\rho$), and rms charge radius ($\langle r_C^2 \rangle$). These observables are defined by the Sachs form factors given in Eqs. (15)–(17), where the magnetic moment in nuclear magnetons (μ_N) is given by $\mu_\rho = G_M(0)\frac{M_N}{m_\rho}$, with M_N the physical nucleon mass and (for comparison with lattice data) m_ρ is the ρ mass evaluated at a particular pion mass; the quadrupole moment is given by $\mathcal{Q}_\rho = G_Q(0)/m_\rho^2$; and finally the charge radius is defined by

$$\langle r_C^2 \rangle = -6 \left.\frac{\partial\, G_C(Q^2)}{\partial Q^2}\right|_{Q^2=0}. \quad (40)$$

In Table II we summarize results for the $\langle r_C^2 \rangle$, μ_ρ, and $\mathcal{Q}_\rho$ of the ρ^+ from various theoretical approaches, together with our calculations using the most sophisticated quark-photon vertex of Eq. (26) (BSE + pion cloud). In general including the dressing of the quark-photon vertex by the BSE and the pion cloud increases the magnitude of μ_ρ by 24%, $\mathcal{Q}_\rho$ by 22%, and $\langle r_C^2 \rangle$ by 16% [27].

In comparing our results with lattice QCD we focus on the lattice simulation from Ref. [25], as they extend to the lightest pion mass, namely, $m_\pi = 161$ MeV. Our computations

TABLE I. Parameters of the model together with the effective couplings computed from Eqs. (12) and (13). The masses are in units of GeV, the Lagrangian couplings in units of GeV^{-2}, and the effective couplings are dimensionless.

M	Λ_{IR}	Λ_{UV}	G_π	G_ρ	G_ω	Z_π	Z_ρ	Z_ω
0.4	0.24	0.645	19.04	11.04	10.41	17.85	6.96	6.63

TABLE II. Comparison of the ρ^+ charge radii, magnetic moments in units of nuclear magnetons, and quadrupole moments for various theoretical approaches: phenomenological models [6], constituent quark models [8,9,11–14], QCD sum rules [16,18], Dyson-Schwinger equations [19–22], and lattice QCD [25,26]. The lightest pion mass used in the lattice calculation in Ref. [25] is $m_\pi^2 = 0.026$ GeV^2, whereas for Ref. [26] it is $m_\pi^2 = 0.49$ GeV^2.

Reference	$\langle r_C^2 \rangle$(fm^2)	μ_ρ (μ_N)	$\mathcal{Q}_\rho$ (fm^2)
This work	0.67	3.14	−0.070
Garcia Gudiño [6]		2.6(6)	
Cardarelli [8]	0.35	2.76	−0.024
De Melo [9]	0.37	2.61	−0.052
Melikhov [11]	0.33	2.87	−0.031
Jaus [12]		2.23	−0.022
Choi [13]		2.34	−0.028
Biernat [14]		2.68	−0.027
Samsonov [16]		2.4(4)	
Aliev [18]		2.8(6)	
Hawes [19]	0.37	3.28	−0.055
Bhagwat [20]	0.54	2.54	−0.026
Roberts [21]	0.31	2.14	−0.037
Pitschmann [22]		2.13	
Owen [25]	0.670(68)	2.613(97)	−0.0452(61)
Shultz [26]	0.30(6)	2.00(9)	−0.020(4)

as functions of m_π^2 are performed by keeping the regularization parameters (Λ_{IR} and Λ_{UV}) and the couplings (G_π, G_ρ, and G_ω) fixed, and varying the current quark mass that enters the gap equation. Results for the ρ mass as a function of m_π^2 (or equivalently the current quark mass) are presented in Fig. 6, where we find remarkable agreement between our NJL calculation and the lattice results of Ref. [25].

At the physical pion mass, our values for $\langle r_C^2 \rangle$ (see Table II) differ significantly from the constituent quark models, one of the Dyson-Schwinger calculations, and the result quoted in the lattice QCD computation of Ref. [26]. Better agreement is seen
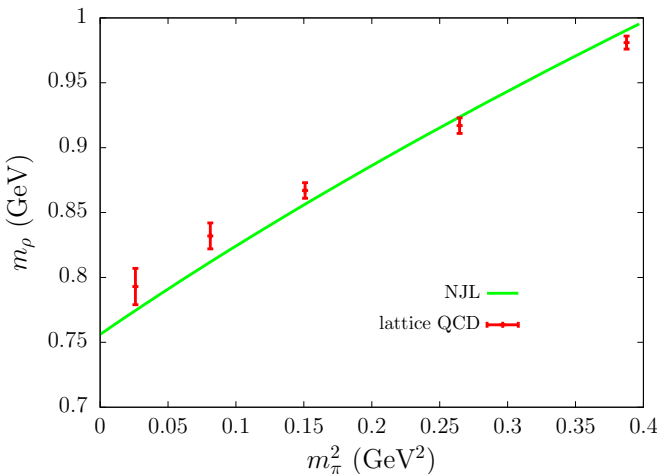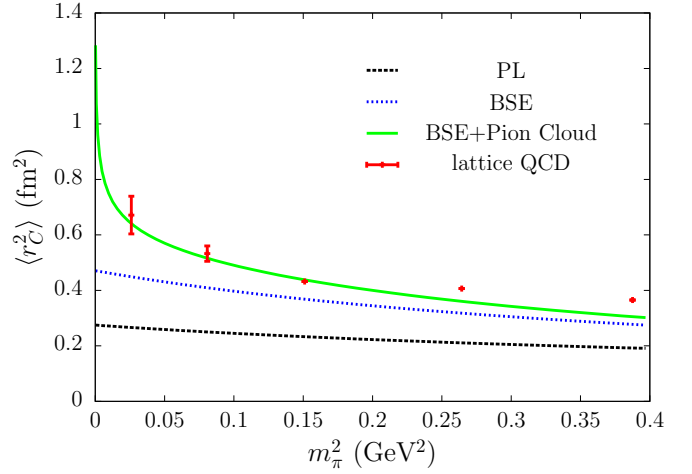

FIG. 7. (Color online) Squared charge radius $\langle r_C^2 \rangle$ for the ρ^+ meson computed using the three levels of sophistication for the quark-photon vertex: pointlike (PL), using the inhomogeneous BSE (BSE), and including the pion cloud (BSE + pion cloud). Comparison is made with lattice results from Ref. [25].

with the Dyson-Schwinger equation calculation of Ref. [20]. Our result for $\langle r_C^2 \rangle$ is, however, very similar to the lattice QCD value obtained in Ref. [25] for a pion mass of around 161 MeV. We see that in Fig. 7 their $\langle r_C^2 \rangle$ lies around 0.67 fm^2, possibly reaching 0.7 fm^2 in the physical limit. On the other hand the lattice QCD simulation of Ref. [26] uses a very large pion mass of 700 MeV, which explains its lower value for $\langle r_C^2 \rangle$, evident from the m_π^2 dependence of the lattice points in Fig. 7. The dependence of $\langle r_C^2 \rangle$ on m_π^2 in our NJL calculation, once the inhomogeneous BSE and pion cloud contributions have been included, shows remarkable agreement with the lattice results of Ref. [25]. One sees that the pion cloud contributions have become negligible for $m_\pi^2 \gtrsim 0.4$, GeV^2.

For the ρ^+ magnetic moment (μ_ρ) the values (in units of nuclear magnetons) obtained by the constituent quark models are consistently smaller than our result of $\mu_\rho = 3.14\,\mu_N$, the closest being $\mu_\rho = 2.87\,\mu_N$ from Ref. [11]. The earlier Dyson-Schwinger equation study in Ref. [19] shows good agreement with our work. For the lattice simulation of Ref. [25] the discrepancy with our result is sizable near the physical limit. However, the evolution of our result with m_π^2 shown in Fig. 8 is in good agreement with the lattice QCD calculations except at their lightest pion mass. The larger discrepancy between the model and the lattice data at that lowest value of m_π^2 is most likely a finite volume effect, since $m_\pi L < 4$ [44]. Again, as in the case of $\langle r_C^2 \rangle$, the effect of the large m_π in Ref. [26] is to produce a small value of μ_ρ, as evident from Fig. 8.

Finally we find a large quadrupole moment comparable to the Dyson-Schwinger equation results of Roberts *et al.* [21] and Hawes and Pichowsky [19]. The lattice QCD result of Ref. [25] is ∼30% smaller than our result near the physics point, as illustrated in Fig. 9. However, to determine the reason for the difference, we suggest that it may be worthwhile to investigate the effect of the lack of spherical symmetry on the
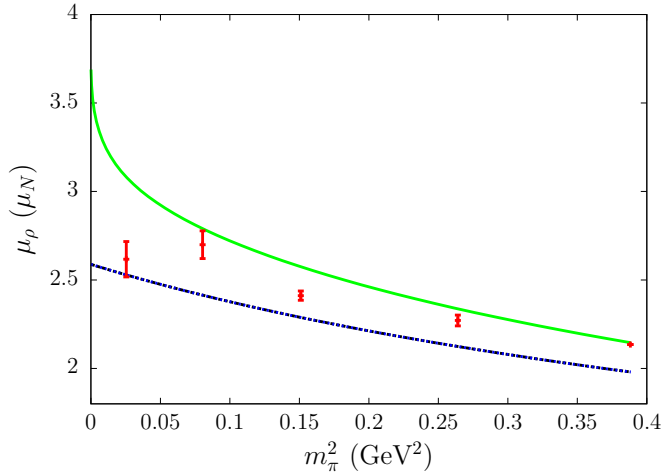

FIG. 6. (Color online) NJL model results for the ρ-meson mass vs m_π^2. Comparison is made with lattice results from Ref. [25].

FIG. 8. (Color online) ρ^+ magnetic moment (μ_ρ) in units of nuclear magnetons vs m_π^2. The curves have the same conventions as Fig. 7.

lattice simulation, considering that the quadrupole moment reflects the shape of the ρ.

Comparison with the lattice simulation of Ref. [25] for the evolution of the ρ^+ Sachs form factors with m_π^2, at a fixed $Q^2 = 0.16$, GeV^2, is made in Figs. 10. The charge form factor G_C is in good agreement with the lattice QCD points, when both the inhomogeneous BSE and pion cloud dressing are included. On the other hand, for the magnetic form factor G_M, the BSE results alone have better agreement with lattice, and the pion cloud causes an overestimate. The deviations are still small, however, considering the simplicity of the calculation. The deviation from the lattice simulation data for G_Q is possibly explained by the same reason behind the disagreement with Q_ρ, that is, the lack of spherical symmetry in the lattice simulation.

A final comparison is made in Fig. 11 for the Sachs form factors as a function of Q^2 for a pion mass of $m_\pi^2 = 0.49$ GeV^2,
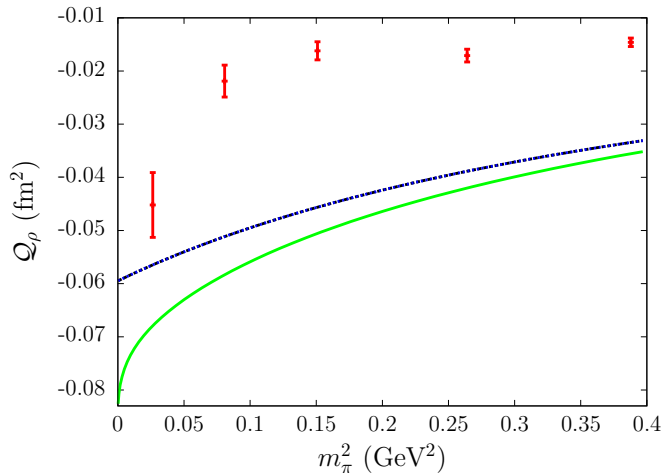

FIG. 9. (Color online) ρ^+ quadrupole moment (Q_ρ) vs m_π^2. The curves have the same conventions as Fig. 7.
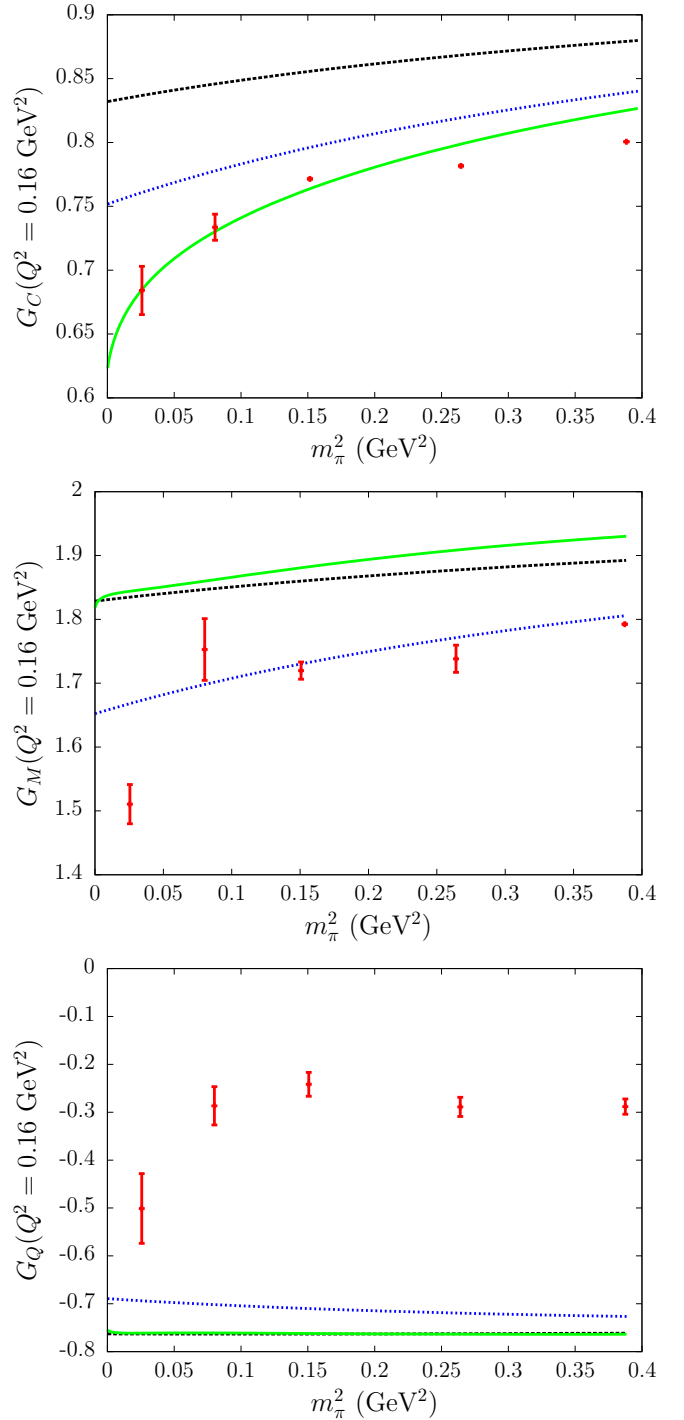

FIG. 10. (Color online) ρ^+ Sachs form factors as functions of m_π^2 at $Q^2 = 0.16$ GeV^2. The curves have the same conventions as Fig. 7.

where the lattice results are from Ref. [26]. We find that our model qualitatively describes the ρ^+ form factors obtained from the lattice computation. Once again the addition of the pion cloud causes an overestimate of $G_M(Q^2)$ and the magnitude of $G_Q(Q^2)$ also appears too large.
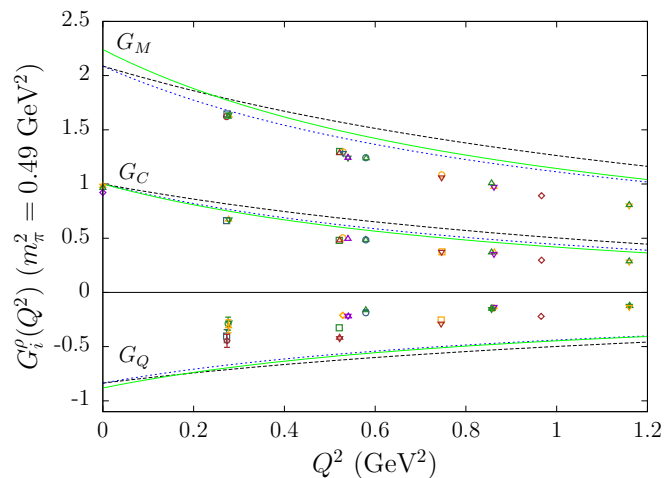
FIG. 11. (Color online) ρ^+ Sachs form factors for $m_\pi^2 = 0.49$ GeV^2. Comparison is made with lattice results from Ref. [26] and the curves have the same conventions as Fig. 7.

V. CONCLUSIONS

We computed the electromagnetic form factors of the ρ^+ meson using an NJL model that simulates aspects of quark confinement. The quark-photon vertex is studied in three levels of sophistication: pointlike dressed quark, via the inhomogeneous BSE, and also including corrections from a pion cloud. The results are qualitatively in good agreement with the recent lattice QCD computations.

The main level of disagreement comes from the quadrupole moment and the corresponding form factor. We suggest that

lattice QCD studies of this type should look at the possible effects of the lack of spherical symmetry of a cubic lattice in the quadrupole moments and form factors. It would certainly be helpful to have further lattice studies over a range of pion masses and momentum transfers. Experimental measurements would also be extremely valuable.

Therefore, the present work on the ρ meson structure and the progress in the computation of the electromagnetic form factors of the π and K, including the pion cloud, reported in Ref. [30], support the importance of the model as a tool to describe hadronic structure. In addition, the NJL model is a quantum field theory where calculations are relatively straightforward and it gives good results when compared to more sophisticated methods that require much more resources, such as lattice QCD. These advantages are useful in order to perform larger calculations in problems such as the description of hadrons in the nuclear medium, as required, for example, to explore the properties of neutron stars. In such cases the NJL model serves as a very useful tool to guide possible future computations of lattice QCD and other more sophisticated approaches.

[1] A. W. Thomas and W. Weise, *The Structure of the Nucleon* (Wiley-VCH, Berlin, 2001).

[2] K. Olive *et al.* (Particle Data Group), Chin. Phys. C **38**, 090001 (2014).

[3] B. Aubert *et al.* (BABAR Collaboration), Phys. Rev. D **78**, 071103 (2008).

[4] A. Dbeyssi, E. Tomasi-Gustafsson, G. I. Gakh, and C. Adamuscin, Phys. Rev. C **85**, 048201 (2012).

[5] C. Adamuscin, G. I. Gakh, and E. Tomasi-Gustafsson, Phys. Rev. C **75**, 065202 (2007).

[6] D. García Gudiño and G. Toledo Sánchez, Int. J. Mod. Phys. Conf. Ser. **35**, 1460463 (2014).

[7] P. L. Chung, F. Coester, B. D. Keister, and W. N. Polyzou, Phys. Rev. C **37**, 2000 (1988).

[8] F. Cardarelli, I. Grach, I. Narodetsky, G. Salme, and S. Simula, Phys. Lett. B **349**, 393 (1995).

[9] J. P. B. C. de Melo and T. Frederico, Phys. Rev. C **55**, 2043 (1997).

[10] H.-M. Choi and C.-R. Ji, Phys. Rev. D **59**, 074015 (1999).

[11] D. Melikhov and S. Simula, Phys. Rev. D **65**, 094043 (2002).

[12] W. Jaus, Phys. Rev. D **67**, 094010 (2003).

[13] H.-M. Choi and C.-R. Ji, Phys. Rev. D **70**, 053015 (2004).

[14] E. P. Biernat and W. Schweiger, Phys. Rev. C **89**, 055205 (2014).

[15] T. M. Aliev, I. Kanik, and M. Savci, Phys. Rev. D **68**, 056002 (2003).

[16] A. Samsonov, J. High Energy Phys. 12 (2003) 061.

[17] V. V. Braguta and A. I. Onishchenko, Phys. Rev. D **70**, 033001 (2004).

[18] T. M. Aliev and M. Savci, Phys. Rev. D **70**, 094007 (2004).

[19] F. T. Hawes and M. A. Pichowsky, Phys. Rev. C **59**, 1743 (1999).

[20] M. S. Bhagwat and P. Maris, Phys. Rev. C **77**, 025203 (2008).

[21] H. L. L. Roberts, A. Bashir, L. X. Gutierrez-Guerrero, C. D. Roberts, and D. J. Wilson, Phys. Rev. C **83**, 065206 (2011).

[22] M. Pitschmann, C.-Y. Seng, M. J. Ramsey-Musolf, C. D. Roberts, S. M. Schmidt, and D. J. Wilson, Phys. Rev. C **87**, 015205 (2013).

[23] W. Andersen and W. Wilcox, Ann. Phys. (NY) **255**, 34 (1997).

[24] J. N. Hedditch, W. Kamleh, B. G. Lasscock, D. B. Leinweber, A. G. Williams, and J. M. Zanotti, Phys. Rev. D **75**, 094504 (2007).

[25] B. J. Owen, W. Kamleh, D. B. Leinweber, M. S. Mahbub, and B. J. Menadue, Phys. Rev. D **91**, 074503 (2015).

[26] C. J. Shultz, J. J. Dudek, and R. G. Edwards, Phys. Rev. D **91**, 114501 (2015).

[27] I. C. Cloët, W. Bentz, and A. W. Thomas, Phys. Rev. C **90**, 045202 (2014).

[28] Y. Nambu and G. Jona-Lasinio, Phys. Rev. **122**, 345 (1961).

[29] Y. Nambu and G. Jona-Lasinio, Phys. Rev. **124**, 246 (1961).
[30] Y. Ninomiya, W. Bentz, and I. C. Cloët, Phys. Rev. C **91**, 025202 (2015).
[31] S. Klevansky, Rev. Mod. Phys. **64**, 649 (1992).
[32] D. Ebert, T. Feldmann, and H. Reinhardt, Phys. Lett. B **388**, 154 (1996).
[33] G. Hellstern, R. Alkofer, and H. Reinhardt, Nucl. Phys. A **625**, 697 (1997).
[34] W. Bentz and A. W. Thomas, Nucl. Phys. A **696**, 138 (2001).
[35] T. Hatsuda and T. Kunihiro, Phys. Rep. **247**, 221 (1994).
[36] U. Vogl and W. Weise, Prog. Part. Nucl. Phys. **27**, 195 (1991).
[37] I. C. Cloët, W. Bentz, and A. W. Thomas, Phys. Lett. B **621**, 246 (2005).
[38] I. C. Cloët, W. Bentz, and A. W. Thomas, Phys. Rev. Lett. **95**, 052302 (2005).
[39] I. C. Cloët, W. Bentz, and A. W. Thomas, Phys. Lett. B **659**, 214 (2008).
[40] W. Bentz, I. C. Cloët, T. Ito, A. W. Thomas, and K. Yazaki, Prog. Part. Nucl. Phys. **61**, 238 (2008).
[41] H. H. Matevosyan, W. Bentz, I. C. Cloët, and A. W. Thomas, Phys. Rev. D **85**, 014021 (2012).
[42] M. E. Carrillo-Serrano, I. C. Cloët, and A. W. Thomas, Phys. Rev. C **90**, 064316 (2014).
[43] Z.-W. Liu, M. E. Carrillo-Serrano, and A. W. Thomas, Phys. Rev. D **91**, 014028 (2015).
[44] C. Gattringer and C. B. Lang, Lect. Notes Phys. **788**, 1 (2010).